Thermospheric Wind Velocity Reconstruction from Remote Sensing data using Curvature and Gradient Regularized Geophysical Inversion Technique

John Elliott, Mark Conde

Motivation:

The Geophysical Institute of the University of Alaska Fairbanks has deployed two networks of all-sky Fabry–Pérot interferometers known as Scanning Doppler Imagers (SDIs). These instruments measure temperature and line of sight (LOS) wind speed in the thermosphere by recording the Doppler spectra of light emitted by airglow and aurora. With a network of these measurements being collected we can infer the wind velocity field in the thermosphere above the ground instruments.

With multiple LOS measurements in a variety of look directions, velocity fields can be reconstructed in 3 primary ways: 1) direct trigonometric calculation 2) basis function fitting and 3) geophysical inversions. While direct trigonometric calculation shows smaller scale structure, the reconstruction can be noisy and are only possible in limited geographic regions. The basis function method reasonably reconstructs large scale structure. But, if enough terms are included to resolve small-scale structures in regions where the observation require it, then obviously unphysical artifacts tend to arise in regions where solutions are poorly constrained by the data. . Figure 1 shows an example of the current capabilities of these two approaches. The third method of geophysical inversion is now being explored as a means to tune a reconstruction that allows small scale structure to be resolved in places with adequate observational coverage, while relaxing back to lower resolution in regions of sparse data coverage.

It is our goal to show that with proper regularization the geophysical inverse technique can be used to capture small scale nuance wherever possible, while still providing useful information over a larger reconstruction region.

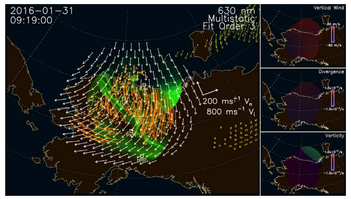

Figure 1: Several methods for wind reconstruction shown. Orange arrows represent direct trigonometric calculation, white arrows represent basis function fit, and green band is Aurora Borealis accelerating ions (ion winds are yellow arrows) which are in turn dragging the neutral winds and establishing small scale structure.
Photo Credit: Mark Conde, UAF Geophysical Institute

Our Phenomena: Airglow

Airglow and aurora (shown right) are diffuse optical emissions originating from various atomic and molecular species in the upper atmosphere. During the day these emissions are not readily visible from the ground because direct and scattered sunlight overwhelms the far weaker atmospheric emissions. Nighttime observations do not suffer from this, but high sensitivity equipment is needed to observe them due to their low brightness.

For our purposes we are interested in night-time airglow originating from atomic oxygen, and in particular the 630 nm emission that originates from around 240 km altitude.

Figure 2: Milky Way, lightning, airglow—Kiribati, central Pacific Ocean. Airglow is present as red light.
Photo credit : Earth Science and Remote Sensing Unit, NASA Johnson Space Center.[1]

1) http://eol.jsc.nasa.gov/SearchPhotos/photo.pl?mission=ISS044&roll=E&frame=45215

Our Instrument: Scanning Doppler Imager
(an Allsky Fabry–Pérot interferometer)

Figure 3: Upper Left: Toolik Field Station, AK SDI getting field maintenance during the summer off-season. Upper Right: Kaktovik, AK SDI around winter solstice. Lower Left: The upper assembly of our SDI at Kaktovik, AK.
Photo Credit: John Elliott

Observational data for this work were acquired using a spectrometer based on a Fabry-Perot etalon and optimized for remote sensing of thermospheric wind and temperature fields. Its salient features included a low-light imaging detector with high time resolution, a capacitance-stabilized etalon capable of piezo-electric separation scanning at 5 Hz or faster, and wide-angle fore optics arranged to place a sharp image of the sky onto the detector (Conde & Smith, 1995, 1997, 1998)[1]. The instrument resolves the sky scene into a software-defined set of sub-regions, and compiles a high-resolution Doppler spectrum of the source illumination originating from each one. These spectra typically span a wavelength interval of around 10 picometers, and are used to infer Doppler shifts and Doppler widths of the illumination, which are in turn used to infer winds and temperatures at the height of the atmospheric optical emission layer. In recent versions of these instruments the field-of-view is typically divided into 115 sub-regions, and it extends from the zenith down to about 20 degrees to 25 degrees elevation angle. Thus, when observing the 630 nm emission, winds and temperatures are measured in a region that is around 1100 km in diameter.

1)Conde, M., and R. W. Smith, Mapping thermospheric winds in the auroral zone, Geophys. Res. Lett., 22, 3019-3022, 1995.
Conde, M., and R. W. Smith, Phase compensation of a separation scanned, all-sky imaging Fabry-Perot spectrometer for auroral studies, Appl. Opt., 36, 5441-5450, 1997.
Conde, M., and R. W. Smith, Spatial structure in the thermospheric horizontal wind above Poker Flat, Alaska, during solar minimum, J. Geophys. Res., 103, 9449-9472, 1998.

The Geophysical Inversion:

The technique is applicable to scenarios in which a measurement vector **d** can be expressed as a product of a transform **A** multiplied by the physical quantities of interest **v**, i.e., **d=Av**. If the problem is bijective (and a few other niceties) we can invert our problem such that our unknown vector **v** can be found as $\mathbf{A}^{-1}\mathbf{d} = \mathbf{A}^{-1}\mathbf{A}\,\mathbf{v} = \mathbf{v}$. We then only need to invert **A** and apply it to **d** to find our vector **v**.

In practice these transforms are of under determined by the data and possibly ill posed. What this means is that the reconstruction is not unique and multiple (possibly infinite) reconstructions can solve this problem. Thus, we introduce some additional constraints in order to provide a unique and physically plausible solution. Adding such constraints is known as regularization.

Harding et. al.[1] presented an implementation of this approach applied specifically to the problem of inferring two-component horizontal thermospheric wind vectors **v** from observations **d** that only give a single line of sight component. Constraints are obtained because the high kinematic viscosity and convective stability of the the thermosphere does not allow winds with extreme curvature or extreme gradient. Following the method of Tikhonov Regularization (ridge regression), we can identify our regularization parameter as $\mathbf{R}=\lambda_0(\mathbf{G}^T\mathbf{G} +\lambda_1\mathbf{C}^T\mathbf{C})$, where **G** and **C** represent gradient and curvature respectively. We have introduced two hyper parameters to scale the ratio of regularization desired for each component, λ_1, and the overall regularization of both, λ_0. Thus with **R** defined we can apply the tools of Tikhonov Regularization to find our analytical solution to our regularization problem: $\mathbf{v^*} = (\mathbf{A}^T \mathbf{\Sigma}^{-1} \mathbf{A} + \mathbf{R})^{-1}\ \mathbf{A}^T \mathbf{\Sigma}^{-1} \mathbf{d}$.

With our approximate wind field solution found from Tikhonov regularization, we now seek to optimize our hyper parameters. Harding et. al.[1] has proposed a mechanism for determining these values. They propose to allow a balance of gradient and curvature regularization that is not the minimum of their cost function (||data|| + ||regularization||), but rather the geometric mean. We have modified our reconstruction to encapsulate this desired balance, and further constrain our hyper parameters to the open set (0,1) such that: $\mathbf{R}=\lambda_0((1-\lambda_1) * \mathbf{G}^T\mathbf{G} +\lambda_1\mathbf{C}^T\mathbf{C})$ and $\mathbf{v^*} = ((1-\lambda_0) * \mathbf{A}^T \mathbf{\Sigma}^{-1} \mathbf{A} + \mathbf{R})^{-1}\ \mathbf{A}^T \mathbf{\Sigma}^{-1} \mathbf{d}$. With these modifications, we find a reasonable set of values for our λ_l by means of brute force searching and manually picking final values.

Future work will be to automate this relationship by comparing the data cost and curvature cost (Harding 2015) and later to investigate localization of parameters instead of implement them on a global scale, in order to maintain large scale usability and find small scale structure. This would change our λ_l from scalar valued to matrices, allowing us to weight the localized curvature and gradient regularization based on suitable metrics.

1) Harding, B. J., J. J. Makela, and J. W. Meriwether (2015), Estimation of mesoscale thermospheric wind structure using a network ofinterferometers, J. Geophys. Res. Space Physics, 120, 3928–3940, doi:10.1002/2015JA021025.

Results: (so far)

The current status of this effort is that we have a functional initial algorithm, strongly derived from the work of Harding et. al. We have implemented a parameterized curvature and gradient regularized Tikhonov inversion and begun work on optimizing our hyper parameters automatically. With “best guess” tuning of hyper parameters we test our algorithm with synthetic wind measurements generated by taking the real instrument transform from our Alaskan network and applying it to a constant wind field of (100,100,0) m/s with a 5% Gaussian noise introduced.

The results (Figure 4) show our synthetic wind reconstructed. There are artifacts present in the northern regions regardless of instrument transform that will need addressed in later revisions. These artifacts likely are due to the construction of the regularization or instrument transform, but at this time the source is not known. When the meridional, zonal, and vertical wind vectors are reconstructed and analyzed with the original winds, ringing is present in the reconstruction and a tendency to overdamp is also noticeable.

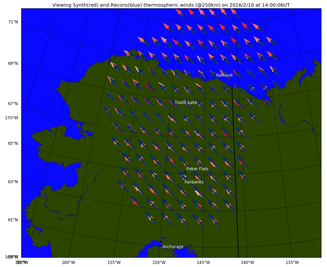

Figure 4: Synthetic winds (red arrows) are compared with the geophysically inverted reconstruction (blue arrows). Extreme northern region and southern region find disagreement on magnitude of wind but not direction.

When we apply the inversion to real data (same data as figure 1, shown Figure 5) in our Alaskan SDI network, we find our results broadly in agreement with other current methods. Attempts to ease the regularization and capture finer structure initially show success, but more investigation is necessary to better tune hyper parameters to capture all potential structure.

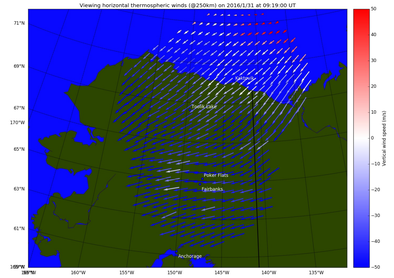

Figure 5: 2016/01/31 at 9:00 UT thermospheric winds are reconstructed over Alaska using the described geophysical inversion